In Vivo Imaging of Cardiac Related Impedance Changes

B. Murat Eyüboğlu, Brian H. Brown and David C. Barber
The University of Sheffield
Department of Medical Physics and Clinical Engineering
Royal Hallamshire Hospital

ELECTRICAL IMPEDANCE TOMOGRAPHY (EIT) produces cross-sectional images of the electrical resistivity distribution within the body, made from voltage or current measurements through electrodes attached around the body. The electrical resistivity of different biological tissues ranges from 0.65 Ωm for cerebrospinal fluid (CSF), increasing through blood, muscle and fat, to 166 Ωm for bone [1]. As a result of this wide range, reasonably good soft tissue contrast can be achieved by impedance imaging. Variations in tissue resistivity associated with physiological events, such as cardiac and respiratory activity, allows EIT to produce functional images. This technique has the advantages of not involving any ionizing radiation and being very much cheaper than other CT techniques, but the disadvantage of offering only poor spatial resolution [2]. Several reviews on electrical impedance imaging have recently appeared [1, 3–5]. The first in vivo EIT images were produced in 1983 at the University of Sheffield [6] with a system that was called "applied potential tomography" (APT). A review of possible clinical applications of APT has been given in a previous paper [7], as development of this new technique by many research teams continues [8].

The electrical resistivity of blood at body temperature (typically 1.5 Ωm) is well separated from the resistivity of other tissues [1]. Therefore, the resistivity of most tissues changes significantly with blood perfusion of the tissue. In 1932, Atzler and Lehmann [9] recorded the variations in capacitance of a human thorax with their dielectrography equipment and related the impedance changes to the mechanical activity of the heart. Following this, Nyboer et al. [10] recorded the variations in human thoracic impedance to high frequency electrical current during the cardiac cycle. Patterson et al. [11] developed a four-electrode technique to measure the thoracic impedance, and Kubicek et al. [12] introduced a technique called impedance cardiography (ICG) to calculate the cardiac output (CO) from a four-electrode impedance measurement. Mohapatra [13] has published a review on the use of the electrical impedance technique to monitor cardiac activity. The global impedance waveforms measured by the four-electrode technique contain contributions from many sources. Following the rapid ejection of blood from the ventricles, the conductivity distribution within the thorax changes very rapidly with flow of blood to both systemic and pulmonary circulations and to various tissues within the thorax. The relative contribution of each area of the global impedance cardiograph is a subject of continuing research. However, it has been shown that the thoracic resistivity variations during the cardiac cycle can be imaged by ECG-gated EIT, and the variations can be localized from these images [14, 15].

EIT is based on the fact that current flow in a volume conductor results in a voltage distribution that is a function of the conductivity distribution within the conductor. The relation between this potential distribution and the distribution of conductivity, $\sigma(x, y, z)$, and permittivity, $\epsilon(x, y, z)$, within a source-free medium can be expressed as:

$$\nabla \cdot (\gamma \nabla \Phi(x, y, z)) = 0$$

with boundary condition:

$$J = \gamma \frac{\partial \Phi(x, y, z)}{\partial n}$$

where $\Phi(x, y, z)$ is the electrical potential at a point (x, y, z) within the conducting medium; J is the outward normal component of the electric current density vector at the surface; $\partial/\partial n$ is the normal derivative to the surface; and $\gamma = \sigma + j\omega\epsilon$ (where ω is an angular frequency). If the frequency of the applied current is sufficiently low, then static electric current ($\omega = 0$) can be assumed; or if a purely resistive impedance distribution ($\epsilon = 0$) is assumed (although in some tissues, such as lung tissue, there is a significant displacement current), then $\gamma(x, y, z) = \sigma(x, y, z)$. Given the conductivity distribution $\sigma(x, y, z)$ and the current density at the electrodes, the potential distribution can be calculated. This procedure is known as the forward problem. In the case of EIT, the conductivity distribution is unknown and needs to be determined. Knowing a complete set of applied currents and the corresponding peripheral voltage profiles, the resistivity distribution within the volume conductor can be calculated by solving the inverse problem [16]. Hence, resistivity maps (images) of the region can be reconstructed. To achieve this, a system to scan the applied current and measure the voltage profiles around the periphery and an algorithm to reconstruct an image of the resistivity distribution from the measured profiles are required.

This article describes a gated EIT system to image the cardiogenic electrical resistivity variations and the results of in vivo studies on human subjects.

DATA COLLECTION HARDWARE

Figure 1 is a block diagram of the ECG-gated electrical impedance tomography system. A 50 kHz 5 mA (peak-to-peak) current is applied, in turn, between all adjacent pairs (which are named as drive pairs) of the 16 electrodes attached on the surface in the transverse plane of the body. Potential differences (gradients) between an independent set of adjacent electrode pairs (receive electrode pairs) are measured. The number of independent measurements is limited by the number of electrodes. With N electrodes, using the principle of superposition, only $(N - 1)$ independent voltage measurements can be made for each current-drive pair. This results in $N * (N - 1)$ measurements. It follows from the reciprocity theorem that reciprocal measurements should be equal [17, 18]. The number of possible independent measurements is therefore equal to $N * (N - 1)/2$. However, if one of the measurement electrode pairs is also a current-drive electrode, the voltage drop across the contact impedances will also appear in the measured voltage. If these measurements are removed, then for N electrodes there are only $N * (N - 3)/2$ actual independent measurements. With 16 electrodes, this gives $(16 * 13)/2 = 104$ independent measurements, which will be referred to in this paper as a "data cycle." Several data cycles can be averaged to improve signal-to-noise ratio (S/N); this averaged data set is called a "frame," and a single image can be reconstructed from these data [19, 20]. Each measurement takes 390 μs; with 16 electrodes this gives a frame rate of approximately 24 frames per second, which offers adequate temporal resolution for cardiac imaging [21, 22]. A 17 th electrode is

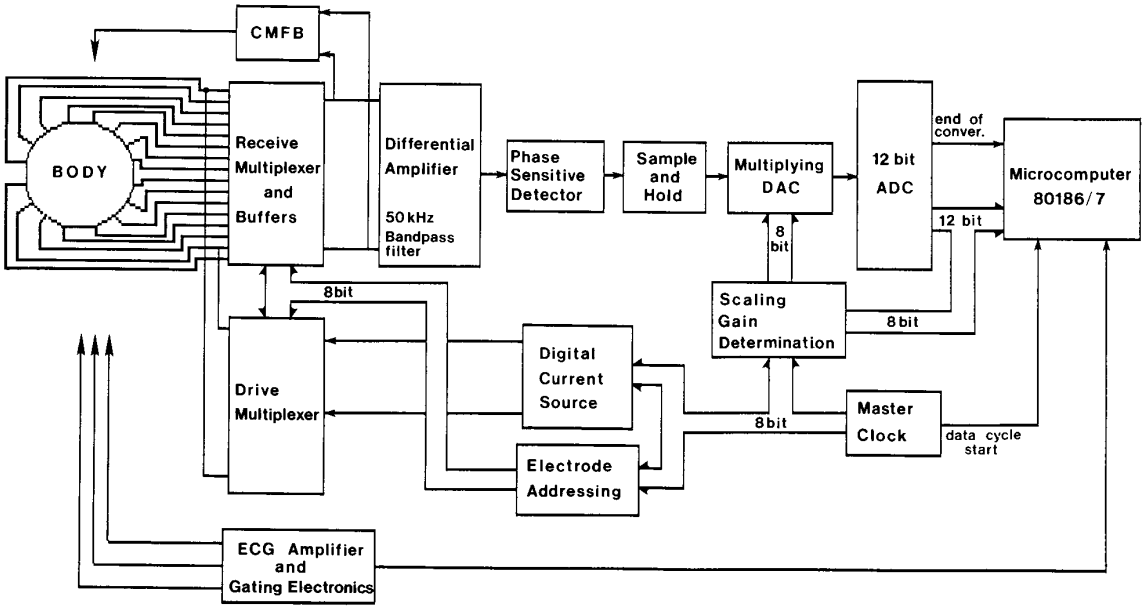

Figure 1. Block diagram of the ECG-gated electrical impedance tomography system.

used for common-mode feedback (CMFB).

The dynamic range of the peripheral potential gradient profile is 40:1 for 16 electrodes placed around a cylindrical conductor (i.e., the potential gradient recorded from an electrode pair adjacent to the drive pair is 40 times larger than that obtained on the opposite side of the cylindrical conductor [23]). To achieve optimum S/N ratio, the potential gradients are normalized using a scaling gain (multiplying digital-to-analog converter (DAC)). This step also makes best use of the dynamic range of the 12-bit analog-to-digital converter (ADC). Because of the human body's inhomogeneity, anisotropy and complex shape, it is impossible to calculate scaling factors for normalization that can give a dynamic range close to 1:1 for different patients. Therefore, for each patient, scaling factors are determined by using a set of potential gradients measured just before the actual data collection starts. These scaling factors are stored into a RAM. Cardiac-related changes are as small as 0.1 percent of some of the differential voltages measured on the periphery. Scaling is therefore vital for the detection of these small variations. After scaling, the measured profile is transfered via an ADC to an Intel 80186 based microcomputer for further processing.

EGG-GATED TEMPORAL AVERAGING

The average resistivity of lung tissue increases with the amount of air inspired. Witsoe and Kinnen [24] have measured an approximately 300 percent increase (from about 7 Ωm to 23 Ωm) in the resistivity of lungs from maximal expiration to maximal inspiration in dogs. The resistivity of lung tissue also changes with the perfusion of blood following ventricular systole, since the resistivity of blood (1.5 Ωm) is significantly lower than that of lung tissue. This change has been calculated as 3 percent [25]. Cardiac-related variations in the measurements may be as small as the input noise level of the front-end electronics. Therefore, to pick up the cardiac-related resistivity variations within the thorax during normal breathing, the respiratory component and the noise must be eliminated. Respiration (typically 12 cycles per minute) and cardiac activity (72 beats per minute) are well separated in frequency. The respiratory component may be rejected by temporal averaging. However, there is evidence for some synchrony of the cardiac and respiratory cycles since they both form part of a common biological system [26–29]. The significance of this synchrony can only be determined experimentally by measuring the amount of noise reduction after temporal averaging. Experience has shown that averaging over at least 100 cardiac cycles is needed during shallow breathing to attenuate the respiratory component and to improve S/N ratio. Cardiac gating is required, not only to eliminate respiratory interference and random noise when imaging the heart and pulmonary perfusion, but also to image the pulsatile movement of blood in other parts of the body.

The ECG of the patient is recorded by an isolated input differential amplifier, and a trigger pulse is produced at the rising edge of each *R*-wave. This pulse sets a gating flag which is sampled by the microcomputer in parallel with the output of the ADC. Following detection of an *R*-wave, 255 successive data cycles (a block of data) are collected. A flowchart of the gated data collection software, which is written in 80186 assembly language and Fortran-77 is given in Fig. 2. Each block of data is collected and stored in the assembly language routine. Data cycles during which an *R*-wave occurs are also found and their positions recorded. After the collection of each block of data, corresponding data cycles before (4 data cycles) and after (26 data cycles) each *R*-wave are averaged. This process is repeated until averaging over 100 cardiac cycles is completed. Since an *R*-wave may occur during any of 104 measurements within the data cycle, a ± 20 ms jitter occurs. On the other hand, this kind of gating does allow us to collect data both before as well as after cardiac systole.

IMAGE ACQUISITION

Several research teams have proposed different algorithms for the reconstruction of resistivity distribution images from measured peripheral data, as recently reviewed [4–5]. Most of these methods are based on an iterative solution of the nonlinear field equations.

The filtered back projection technique used in this study has been explained previously [19, 20]. The major problem with impedance imaging is that the current flow paths are non-linear and a function of the conductivity distribution within the medium. Therefore, back projection over straight

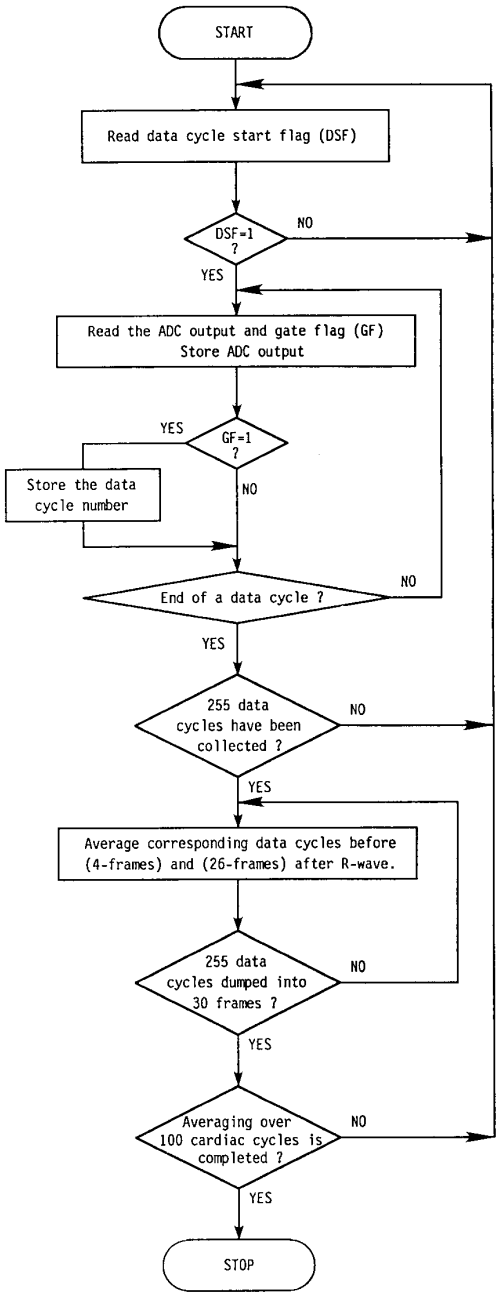

Figure 2. Flowchart of the ECG-gated data collection and temporal averaging software. DSF is the data cycle start flag which is set to "1" at the beginning of each data cycle; GF is the gate flag which is set to "1" when an *R*-wave occurs.

lines, as in the case of X-ray CT, results in significant distortion in the reconstructed image. The algorithm used in this study back projects the voltage gradients measured onto the boundary along curved equipotential lines that are calculated for a circular homogeneous and isotropic region. The back projection method requires two sets of data to reconstruct an image. One set is assumed to be for the case of a homogeneous and isotropic conductivity distribution, which is called the reference frame. Images represent the natural logarithm of the deviation of resistivity distribution from this reference frame.

Although the images are two-dimensional, data measured from the electrodes attached around a volume conductor contain contributions from three dimensions due to the volumetric current flow. Sensitivity is a maximum within the electrode plane and falls with radial and longitudinal distance from the electrodes.

Spatial resolution is a function of the number of independent measurements (hence the number of electrodes), the S/N ratio of the measurements, and also the particular resistivity distribution within the volume conductor [2]. Spatial resolution also changes with position within the image, being better close to the electrodes than at the center [2]. It is therefore not possible to give a simple quantitative expression for the spatial resolution. However, an estimate of its limit can be defined in terms of the number of independent measurements. If the "spatial resolution" is defined as the smallest distance required between two independent features in the field of view before they become indistinguishable, then this distance should be equal to the size of a pixel. For N electrodes, $N * (N - 3)/2$ independent pixels can be obtained within the image. Assuming that the pixels of equal size fill the circular image area of unit radius uniformly, then the pixel area is $2\pi/(N(N - 3))$. If square pixels are used, then the spatial resolution will be $[2\pi/(N(N - 3))]^{1/2}$. For 16 electrodes, this will give a spatial resolution of 9 percent of the array diameter. Similarly, for circular pixels the resolution will be $2[2/(N(N - 3))]^{1/2}$ and it will result in a spatial resolution of 10 percent of the diameter for a 16-electrode system. These are, of course, very crude figures. If spatial resolution is defined in a different way, then these figures will also be different [2].

Images are formed in a 16 × 16 matrix format and displayed on a 16 grey-level CRT display unit as a 32 × 32 matrix after smoothing. Quantitative measurements of temporal resistivity changes in a chosen region of the image are obtained by defining a region of interest (ROI) and measuring the average value of the pixels within.

Visual examination of blood perfusion throughout the cardiac cycle can be carried out by displaying sequential images at actual speed in a cine loop.

IN VIVO STUDIES IN HUMANS

In vivo studies on the thorax were carried out on 10 normal male volunteers aged 24 to 50, during shallow breathing in the standing position. Sixteen conductive silicone rubber electrodes, with surface area 150 mm^2, were equally spaced around the thorax at the level of the fourth intercostal space. For common-mode feedback and ECG pick-up, Ag-AgCl ECG electrodes were used. Two studies were carried out on each volunteer. In vivo images of the neck were collected with the same electrodes placed around the neck.

Images were reconstructed relative to a selected reference frame chosen from any point in the cardiac cycle. A frame at end-diastole, when there are minimal changes related to cardiac activity, has been chosen for the images presented in this paper. For comparison, magnetic resonance imaging (MRI) scans were obtained on 3 of the 10 subjects. These images were ECG-gated 210 ms after the *R*-wave, at the same level as the EIT scans of the thorax, and were the result of averaging 256 cardiac cycles.

RESULTS AND DISCUSSION

Throughout the cardiac cycle, the resistivity distribution within the thorax changes considerably due to the perfusion of blood to the various tissues, flow of blood, dilatation of major blood vessels, and also mechanical movement of the heart itself. Figure 3 shows the time variation of the voltages between adjacent electrode pairs attached around the thorax

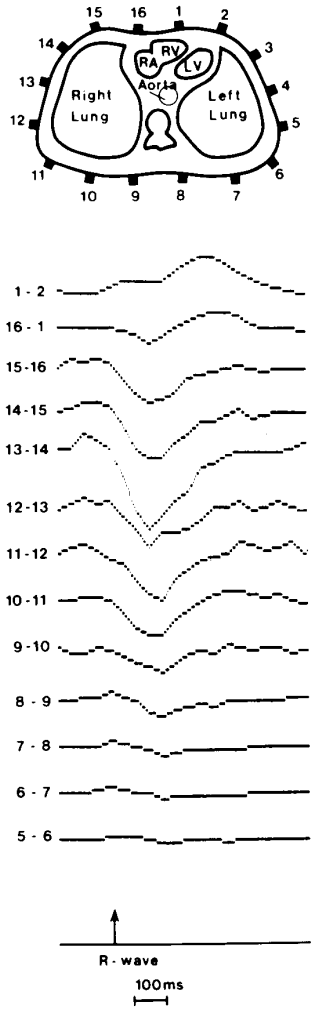

Figure 3. Position of electrodes around the thorax at the 4th intercostal space. (b) Variation of potential gradients between receive electrodes throughout the cardiac cycle, when current flow is applied between electrodes 3 and 4. Receive electrode numbers are shown to the left of each waveform. To reconstruct a sequence of images for one cardiac cycle, 16 of these data sets are required, one for each drive pair.

for a particular current-drive pair. Depending upon the relative position of drive and receive electrode pairs, these variations may have a complicated structure and are difficult to interpret. By scanning the applied current for all independent drive pairs and measuring a profile for each drive ($N * (N - 3)/2$ measurements for N electrodes), EIT has the advantage of producing maps of localized resistivity change. As can be seen from the EIT images of the neck given in Figure 4, the resistivity variations due to about 10 percent dilatation in diameter of the carotid arteries in systole [30] can be imaged. Within a typical thorax of 300 mm diameter, the spatial resolution at its limit should be approximately 30 mm (10 percent of the array diameter), which is sufficient to resolve the heart chambers but not the detail within the chambers.

A set of EIT images over one cardiac cycle and an MRI scan of the same subject are given in Fig. 5. The two ventricles, right atrium, aorta, and two lungs are in the field of view. It must be remembered that these images show temporal variation in resistivity distribution relative to end-diastole.

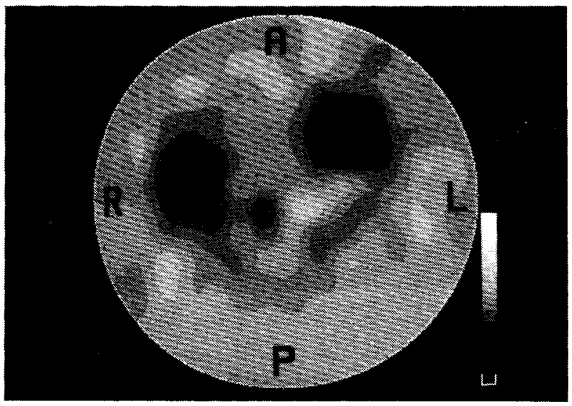

Figure 4. An EIT image of a human neck at peak systole. Dark and bright regions correspond to decreased and increased resistivities relative to end-diastole, respectively. Dilatation of two carotid arteries are seen as decreased resistivities (dark). P, A, L, and R show posterior, anterior, left and right, respectively.

Dark and bright regions correspond to decreased and increased resistivities, respectively. At end-diastole, the ventricles are filled with blood, therefore their resistivities are at their minimum; whereas the aorta, pulmonary arteries, and lungs have their minimum blood content and maximum resistivity. Following ventricular systole, blood is forced into the aorta and pulmonary arteries. With the dilatation of the vessel walls due to this pulsatile flow, their blood volume increases and their average electrical resistivity drops. However, the resistance of both ventricles increases with outflow of blood. This increase in the resistivity of the ventricles takes about a third of the complete cardiac cycle. The resistivity of the lungs decreases gradually with an increase in the amount of blood perfused. As soon as venous return starts, the resistivity of the lungs starts to increase and the resistivity of the atria and the ventricles decreases. Images return to a uniform state towards the end of diastole.

Resistivity variations in five major regions, shown in Fig. 6(a), were investigated. The average of the peak-to-peak percentage resistivity variations, measured from 10 normals over these regions during the cardiac cycle, are given in Fig. 6(a). There are, of course, differences among individuals, and these differences are greater than the differences between repeat measurements. The causes of the differences among individuals needs to be examined. They may be due, in part, to the different size of the ventricles in the field of view for each volunteer, different stroke volumes, and/or the level of the electrodes with respect to the heart.

Figure 6(b) shows the time variation of resistivity in the regions given in Fig. 6(a) for the sequence of Fig. 5. Changes in the heart chambers and aorta lead the changes in the lungs. In this sequence, peak-to-peak variations are about the same for both sides of the heart. However, a notch occurs on the left heart 150 ms after the R-wave. This may be because of some off-plane contributions of volumetric current flow. To have a better understanding of these waveforms, the three-dimensional sensitivity distribution should be studied.

The summation of the average resistivity variations over the regions shown in Fig. 6(a), which represents the variation of global resistivity variation within the field of view, results in a waveform very similar to those obtained in impedance cardiography [12], (Fig. 6(b)). The peak-to-peak variation of this waveform is approximately 0.5 percent of the end-diastolic value. The variation obtained from ICG has been given as less than 0.5 percent (0.1 Ω for 25 Ω resting value) [13].

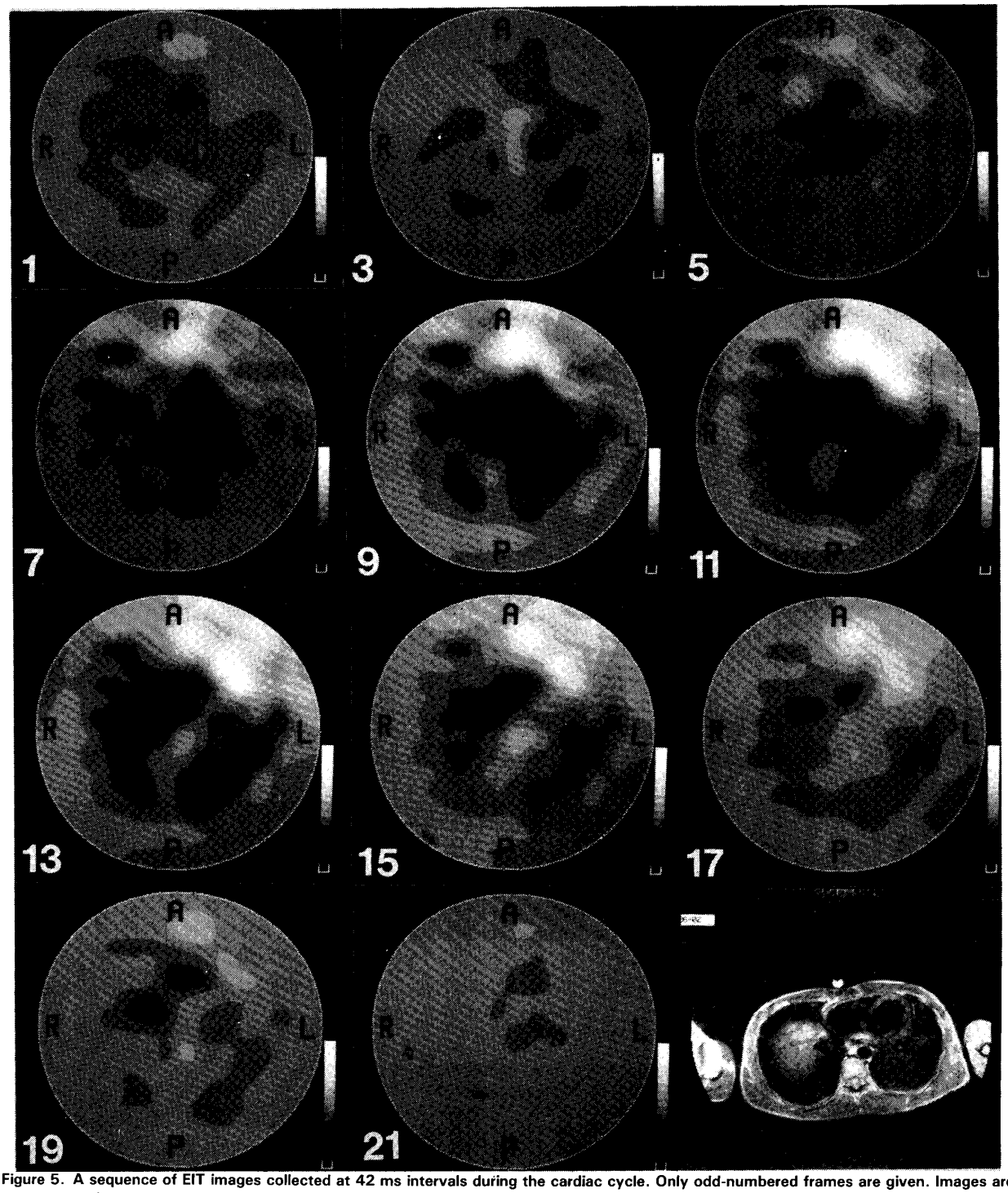

Figure 5. A sequence of EIT images collected at 42 ms intervals during the cardiac cycle. Only odd-numbered frames are given. Images are reconstructed with the reference at end-diastole (frame 4), therefore, all other frames represent the changes in resistivity relative to frame 4. Resistivity of blood is relatively lower than most of the other tissues. Therefore, regions where blood accumulates during systole appear as decreased resistivity (dark) and the regions where blood is removed appear as increased resistivity (bright) in the images. Frames 1 to 3 are towards end-diastole; as all regions approach their reference values (frame 4), the resistivity changes are very small. At frame 4, end-diastole, the ventricles are filled with blood and their resistivity is at its minimum, whereas the resistivity of aorta and lungs is at a maximum. The *R*-wave occurs at frame 5. Following ventricular contraction, the average resistivity of the ventricles starts increasing. During systole, frames 5 to 11, the increase in the resistivity of the ventricles is accompanied by a decrease in the resistivity of the aorta and major arteries due to radial dilatation and the lungs due to perfusion with blood. Frames 12 to 21 belong to diastole; with the return of blood to the ventricles, their resistivity reaches a minimum value and aorta and lungs their maximum values (i.e., to their reference values and hence disappear in the image). Frames 1 and 20 represent approximately the same time in the cardiac cycle. The MRI scan of the same subject, 210 ms after the *R*-wave, is given for comparison in the bottom right corner. Orientation of the MRI image is the same as that of EIT. In the EIT images, the letters P, A, L, and R show posterior, anterior, left and right, respectively.

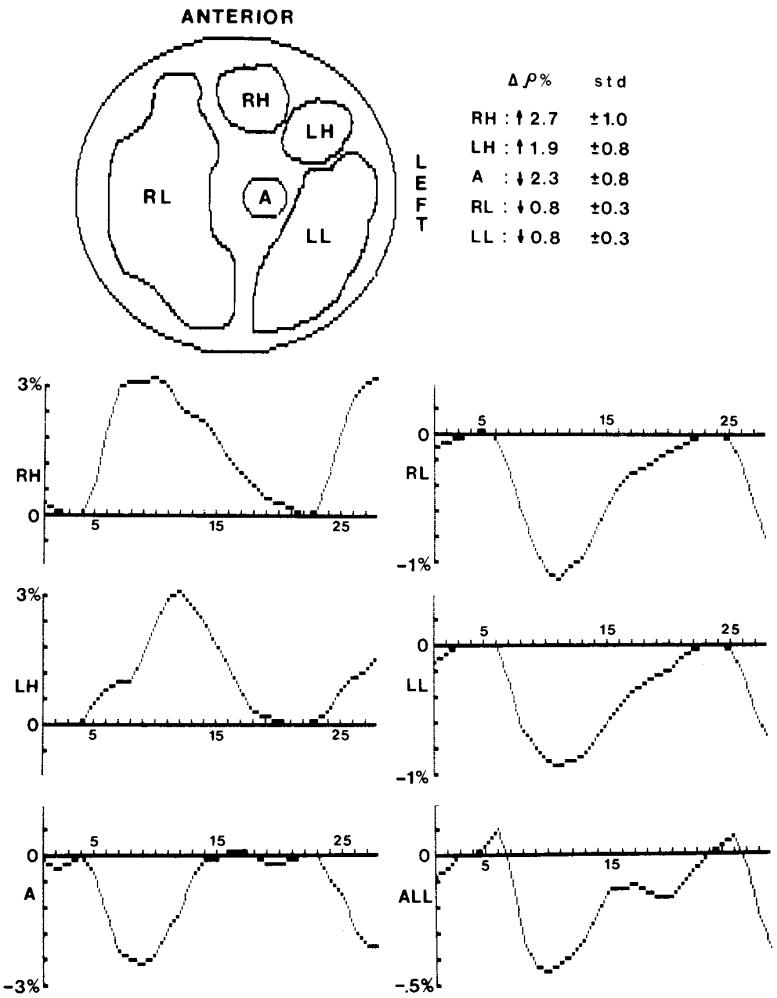

Figure 6. (a) Major regions and the percentage changes in resistivity ($\Delta\rho\%$) over these regions obtained from the EIT images collected from 10 normal subjects. ↑ and ↓ show increase and decrease in resistivity during systole (std is the standard deviation). (b) Time variation of resistivity in the major regions for the sequence of Fig. 5. Letters RH, LH, A, RL, LL are used to show the regions defined as right and left heart, aorta, right and left lung, respectively. The time variation obtained by setting a ROI to cover all the regions shown in (a) is labeled as 'ALL'.

It is attractive to attempt to estimate the blood volume change by using the localized resistivity changes. However, because of the non-uniform and non-linear nature of the sensitivity function and its volumetric distribution, the accuracy of the localized measurements are related to position and the geometry of the regions in which the resistivity changes occur and to the amount of change itself [2]. Therefore, quantitative measurement of the volume variations in the heart chambers needs several assumptions in terms of size and position of the heart. Significant longitudinal motion of the heart during iso-volumetric contraction should also be taken into account. When estimating the pulsatile volume changes in the great blood vessels such as the aorta, the variation of blood resistivity due to flow [31] may also need to be taken into account. The volumetric size of the lungs is large in comparison to EIT's field of view. Therefore, the amount of blood perfusion to the lungs may be determined more accurately.

CONCLUSION

Although as we have shown the spatial resolution is poor and difficult to improve, it is quite clear that the sensitivity of EIT to tissue resistivity variations due to blood perfusion is good enough to image blood flow to the lungs. Hence, abnormalities in pulmonary perfusion, such as pulmonary embolism, should appear in EIT images.

EIT allows us to measure local as well as global resistivity variations. Therefore, more valuable information related to the cardiac activity can be gained from EIT images than from impedance cardiography. It is likely that a cardiac output index may be calculable from the average resistivity variations over the ventricles. However, considerable research is required before the images can be understood in detail. Research is underway to give a better understanding of the sensitivity function and the origin of local variations within the thorax.

EIT may be useful in intensive care units for continuous monitoring of cardiopulmonary function. However, on-line monitoring is not possible with existing equipment because of limitations in image reconstruction speed. With the present system, reconstruction of a single frame takes about 5 seconds. Using parallel processing techniques, reconstruction of images in real-time during the cardiac cycle should be possible. This may bring the possibility of on-line monitoring.

ACKNOWLEDGMENT

The authors wish to express their sincere thanks to the volunteers who took part in this study and to the Department of Medical Illustration, Royal Hallamshire Hospital.

B. M. Eyüboğlu would like to acknowlege the financial support given by a UNESCO fellowship award and an Overseas Research Student (ORS) award from The Committee of Vice-Chancellors and Principals of the Universities of the United Kingdom.

REFERENCES

1. **Barber DC, Brown BH**: Applied potential tomography. *J Phys Sci Instrum*, 17:723-733, 1984.
2. **Seagar AD, Brown BH**: Theoretical limits to sensitivity and resolution in impedance imaging. *Clin Phys Physiol Meas*, 8 Suppl. A:13-31, 1987.
3. **Seagar AD, Barber DC, Brown BH**: Electrical impedance imaging. *IEE Proc*, 134 Pt. A:201-210, 1987.
4. **Yorkey TJ**: *Comparing Reconstruction Methods for Electrical Impedance Tomograpy*. Ph.D. diss., University of Wisconsin at Madison, Madison, WI, 1986.
5. **Yorkey TJ, Webster JG, Tompkins WJ**: Comparing reconstruction algorithms for electrical impedance tomography. *IEEE Trans Biomed Engng*, BME-34:843-852, 1987.
6. **Barber DC, Brown BH, Freeston IL**: Imaging spatial distributions of resistivity using applied potential tomography. *Elec Letts*, 19:933-935, 1983.
7. **Brown BH, Barber DC, Seagar AD**: Applied potential tomography: possible clinical applications. *Clin Phys Physiol Meas*, 6:109-121, 1985.
8. **Brown BH, Barber DC, Tarassenko** (Eds): *Electrical Impedance Tomography—Applied Potential Tomography. Clin Phys Physiol Meas* 8 Suppl A:184, 1987.
9. **Atzler E, Lehmann G**: Über ein neues verfahren zur darstellung der herztätigkeit (dielektrographie). *Arbeitsphysiologie*, 5:636-680, 1932.
10. **Nyboer J, Bango S, Barnett A, Halsey RH**: Radiocardiograms. *J Clin Invest*, 19:773, 1940.
11. **Patterson RP, Kubicek WG, Kinnen E, Noren G, Witsoe D**: Development of an electrical impedance plethymography system to monitor cardiac output. *Proc of 1st Annual Rocky Mountains Conf on Biomed Engng*, Colorado Springs, 1:56-71, 1964.
12. **Kubicek WG, From AHL, Patterson RP, Witsoe DA, Castende A, et al**: Impedance cardiography as a noninvasive means to monitor cardiac function. *J Assoc Adv Med Instrum*, 4:79-84, 1970.
13. **Mohapatra SN**: *Non-invasive Cardiovascular Monitoring by Electrical Impedance Techniques*, Pitman Medical, London, 1981.
14. **Eyüboğlu BM, Brown BH, Barber DC, Seagar AD**: Localisation of cardiac related impedance changes in the thorax. *Clin Phys Physiol Meas*, 8 Suppl A:167-173, 1987.
15. **Eyüboğlu BM, Brown BH, Barber DC**: Imaging cardiopulmonary blood flow using electrical impedance tomography. *Biol Eng Soc Blood Flow 87 Conf*, Leeds, UK, 1987.
16. **Bates RHT**: Full-wave computed tomography; Pt. 1: Fundamental theory. *IEE Proc*, 131 Pt A 8:610-615, 1984.
17. **Geselowitz DB**: An application of electrocardiographic lead theory to impedance plethysmography. *IEEE Trans Biomed Engng*, BME-18:38-41, 1971.
18. **Lehr J**: A vector derivation useful in impedance plethysmographic field calculations. *IEEE Trans Biomed Engng*, BME-19:156-157, 1972.
19. **Barber DC, Brown BH**: Recent developments in applied potential tomography—APT. In: Bacharach S (Ed): *Information processing in medical imaging*, Martinus Nijhoff, Boston, pp 106-121, 1986.
20. **Barber DC, Seagar AD**: Fast reconstruction of resistance images. *Clin Phys Physiol Meas*, 8 Suppl. A:47-54, 1987.
21. **McKinnon GC, Bates RHT**: Towards imaging the beating heart usefully with conventional CT scanner. *IEEE Trans Biomed Engng*, BME-28:123-127, 1981.
22. **Sagel SS, Weiss ES, Gillard RG, Hounsfield GN, Jost RGT**: Gated computed tomography of the human heart. *Investigative Radiology* 12:563-566, 1977.
23. **Brown BH, Seagar AD**: The Sheffield data collection system. *Clin Phys Physiol Meas*, 8 Suppl A:91-97, 1987.
24. **Witsoe DA, Kinnen E**: Electrical resistivity of lung at 100 kHz. *Med Biol Engng*, 5:239-248, 1967.
25. **Pattersonn RP**: Sources of the thoracic cardiogenic electrical impedance signal as determined by a model. *Med Biol Engng Comp*, 23:411-417, 1985.
26. **Guyton AC**: *Textbook of Medical Physiology*, 7th ed, W.B. Saunders, Philadelphia, pp. 153, 472, 513, 1986.
27. **Davies CTM, Neilson JMM**: Sinus arrhythmia in man at rest. *J Appl Physiol*, 22(5):947-955, 1967.
28. **McCrady JD, Vallbona C, Hoff HE**: Neural origin of the respiratory heart rate response. *Am J Physiol*, 211(2):323-328, 1966.
29. **Hirsch JA, Bishop B**: Respiratory sinus arrhythmia in humans: how breathing pattern modulates heart rate. *Am J Physiol*, 241:H620-H629, 1981.
30. **Eriksen M**: Noninvasive measurement of arterial diameters in humans using ultrasound echoes with prefiltered waveforms. *Med Biol Engng Comput*, 25:189-194, 1987.
31. **Lamberts R, Visser KR, Zijlstra WG**: *Impedance Cardiography*, Van Gorcum, Assen, The Netherlands: pp 76- 106, 1984.

B. Murat Eyüboğlu (S'83) was born in Istanbul, Turkey in 1960. He received his B.Sc. in Electrical Engineering and M.Sc. in Electrical and Electronics Engineering from Middle East Technical University (METU), Ankara, Turkey, in 1983 and 1985, respectively. He has been a research assistant at the Department of Electrical and Electronics Engineering of METU since 1983. He has been on leave from METU since November 1985 to the University of Sheffield, where he is studying for a Ph.D. degree. His research is on the development and application of electrical impedance tomography for cardiac imaging.

Mr. Eyüboğlu can be reached at Department of Medical Physics and Clinical Engineering, Royal Hallamshire Hospital, Glossop Road, Sheffield, S10 2JF, U.K.

Brian H. Brown was born in 1941. He received a B.Sc. in Physics from the University of London in 1962 and a Ph.D. in "Waveform Analysis of Nerve and Muscle Action Potentials" from the University of Sheffield in 1969. He was awarded the Founders Prize of the HPA in 1972. Professor Brown was a development engineer with Pye Ltd. and a health physicist at Berkeley Nuclear Power Station. For many years he has worked in the joint University and Health Authority, Department of Medical Physics and Clinical Engineering in Sheffield.

Professor Brown's major interest is in medical electronics involving research and development work on techniques of physiological measurement, the production of instrumentation, and their application to both clinical research and routine patient measurement. His major areas of interest have been the recording of electrical activity from the smooth muscle of the gut, the analysis of nerve action potentials, and the use of electromyography to investigate muscular dystrophy.

In 1977-78 he was sent as a United Nations expert to Hyderabad, India to initiate training courses in medical electronics. His current major research areas are the development of a sensory substitution aid for the profoundly deaf and the practical realization of electrical impedance imaging.

His present address is Royal Hallamshire Hospital, Glossop Road, Sheffield S10 2JF, U.K.

David C. Barber was born in 1944. He graduated from the University of Cambridge with a degree of Natural Sciences in 1966 and then went to London University for an M.Sc. in Radiation Physics and Biology. In 1967 he was an assistant lecturer in the Department of Medical Physics of the University of Aberdeen, where he specialized in nuclear medicine. He became interested in applying digital image processing to radionuclide images and this formed the subject of his Ph.D. thesis "Digital Computer Processing of Radioisotope Scans." In 1971 he moved to the Department of Medical Physics in Sheffield to a Research Fellowship in image processing and in 1975 was appointed a Senior Physicist in the Health Service. He became a Top Grade Physicist in 1985.

Dr. Barber's principal areas of research include the use of factor analysis techniques in the analysis and classification of radionuclide image data and other physiological signals. He has also been interested in the development of a small computer system in nuclear medicine. Since 1981 he has been actively involved (with Professor Brown) in developing an impedance image technique for medical use.